9 Nanoholes array and polarization effect

Contents

- Physical mechanism of single hole
- Fabrication of nanohole array
- Polarization issue of elliptical nanoholes
- Applications of nanoholes

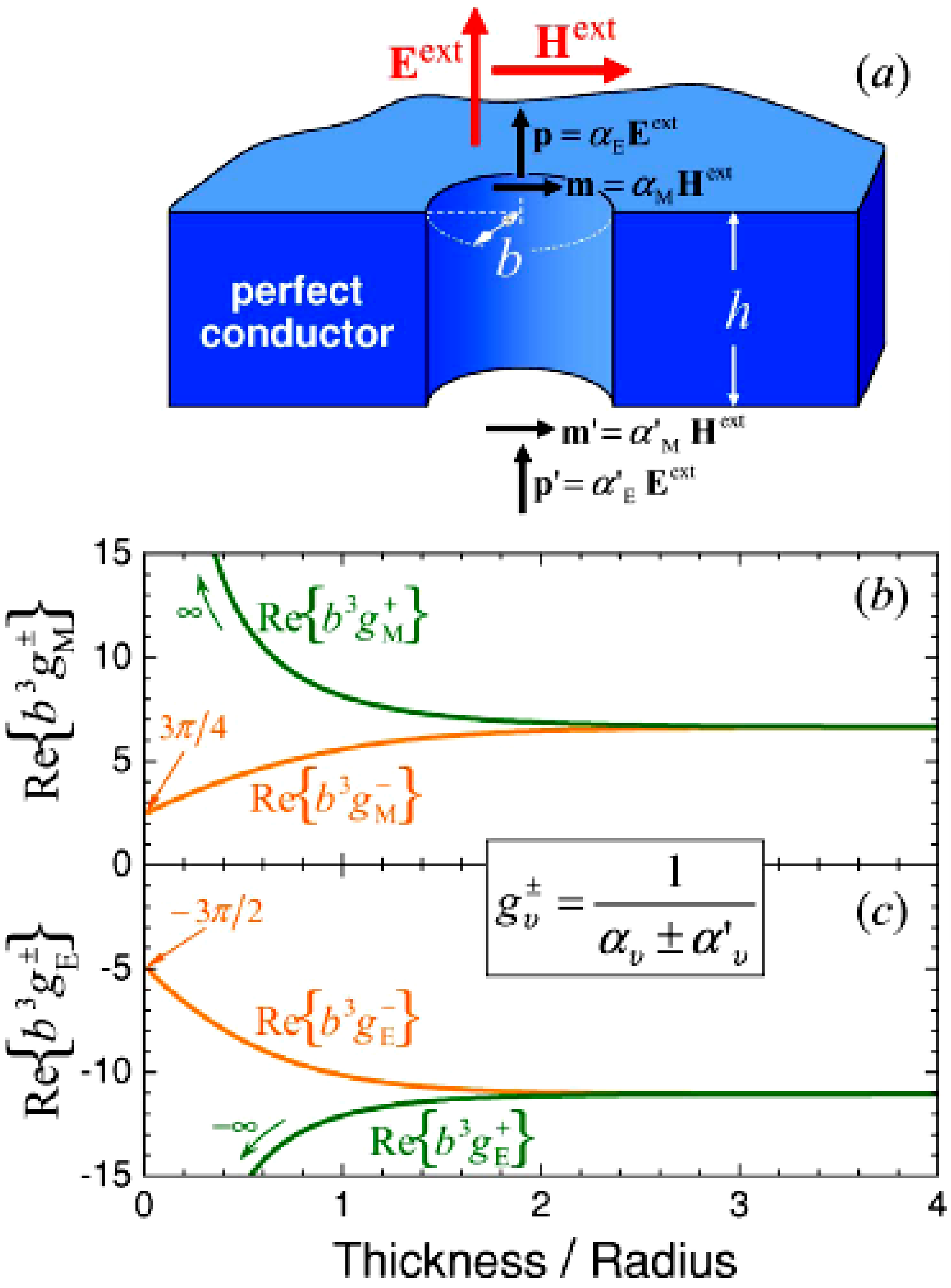

$$p = \alpha_E(E_z^{\text{ext}} + G_{zz}p - Hm) + \alpha'_E(G_{zz}p' - Hm'),$$

$$p' = \alpha'_E(E_z^{\text{ext}} + G_{zz}p - Hm) + \alpha_E(G_{zz}p' - Hm'),$$

$$m = \alpha_M(H_y^{\text{ext}} + G_{yy}m - Hp) + \alpha'_M(G_{yy}m' - Hp'),$$

$$m' = \alpha'_M(H_y^{\text{ext}} + G_{yy}m - Hp) + \alpha_M(G_{yy}m' - Hp'),$$

with a new lattice sum defined as

$$H = -ik \sum_{n \neq 0} e^{-ik_\parallel x_n} \partial_{x_n} \frac{e^{ikR_n}}{R_n}.$$

Review of Modern Physics 79, Oct.-Dec. (2007).

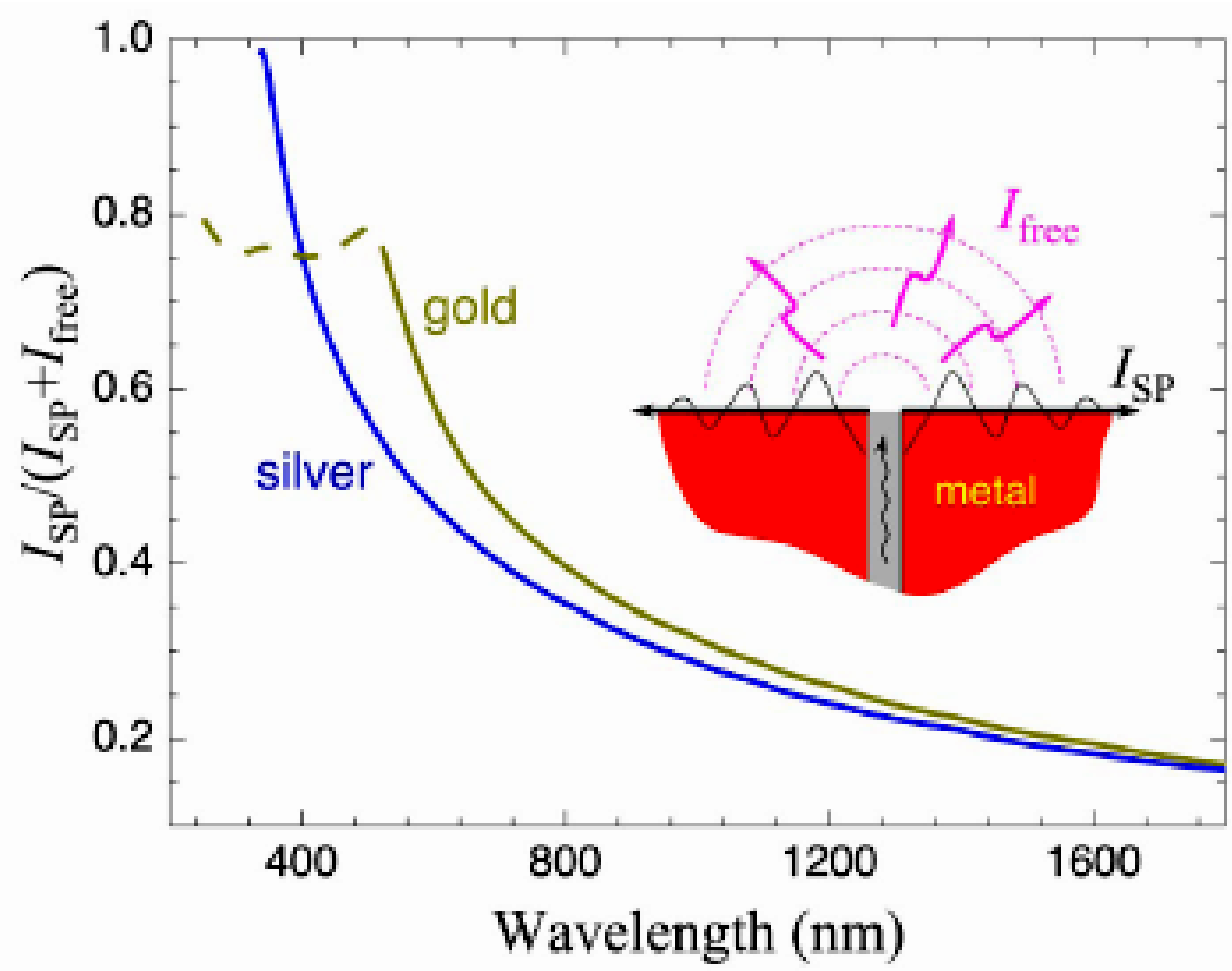

1.0
0.8
0.6
0.4
0.2
400
800
1200
1600
Wavelength (nm)
$I_{SP}/(I_{SP}+I_{free})$
gold
silver
I_{free}
I_{SP}
metal

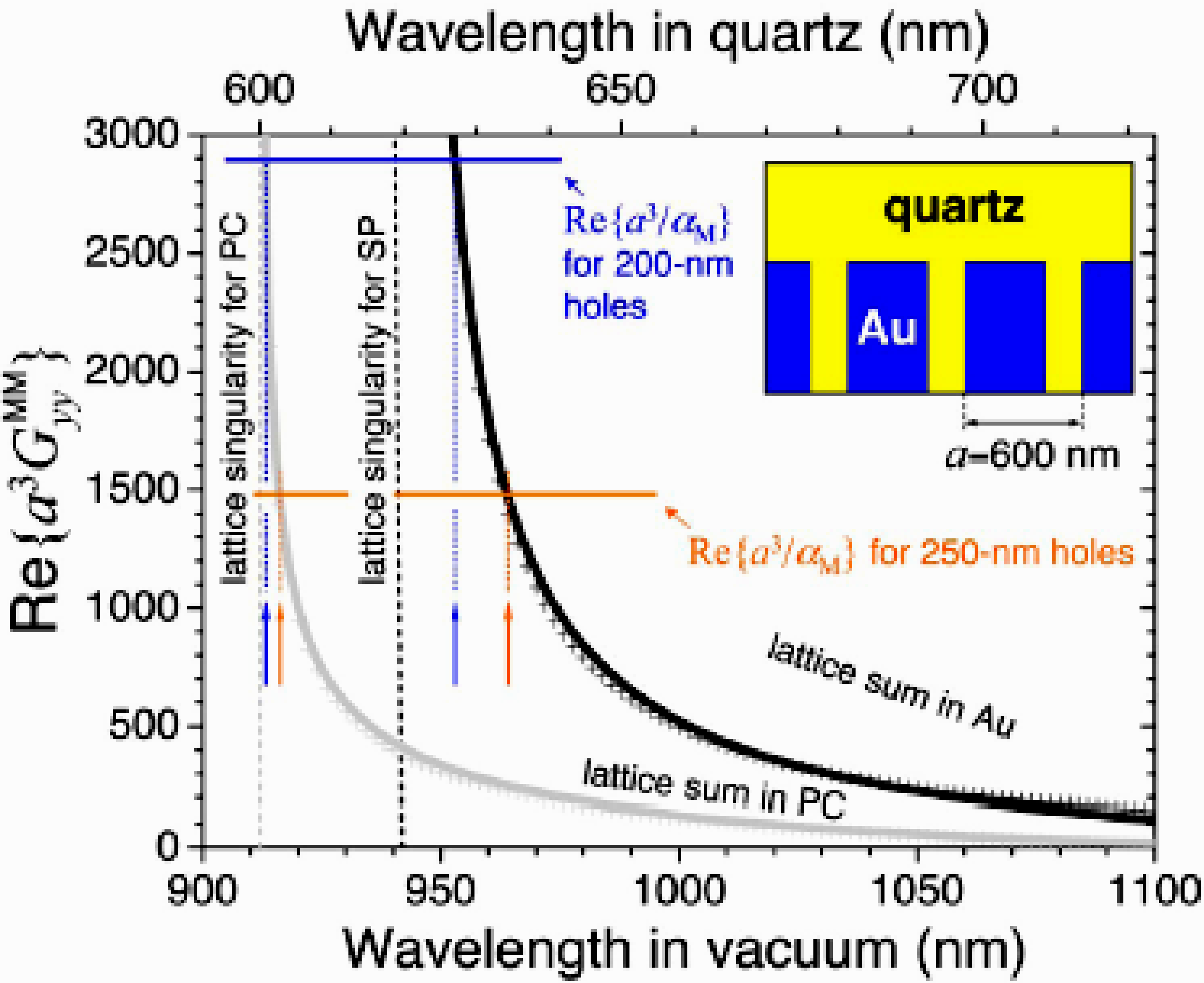

Wavelength in quartz (nm)
600
650
700
3000
2500
2000
1500
1000
500
0
$\mathrm{Re}\{a^3 G_{yy}^{\mathrm{MM}}\}$
lattice singularity for PC
lattice singularity for SP
$\mathrm{Re}\{a^3/\alpha_\mathrm{M}\}$ for 200-nm holes
quartz
Au
a=600 nm
$\mathrm{Re}\{a^3/\alpha_\mathrm{M}\}$ for 250-nm holes
lattice sum in Au
lattice sum in PC
900
950
1000
1050
1100
Wavelength in vacuum (nm)

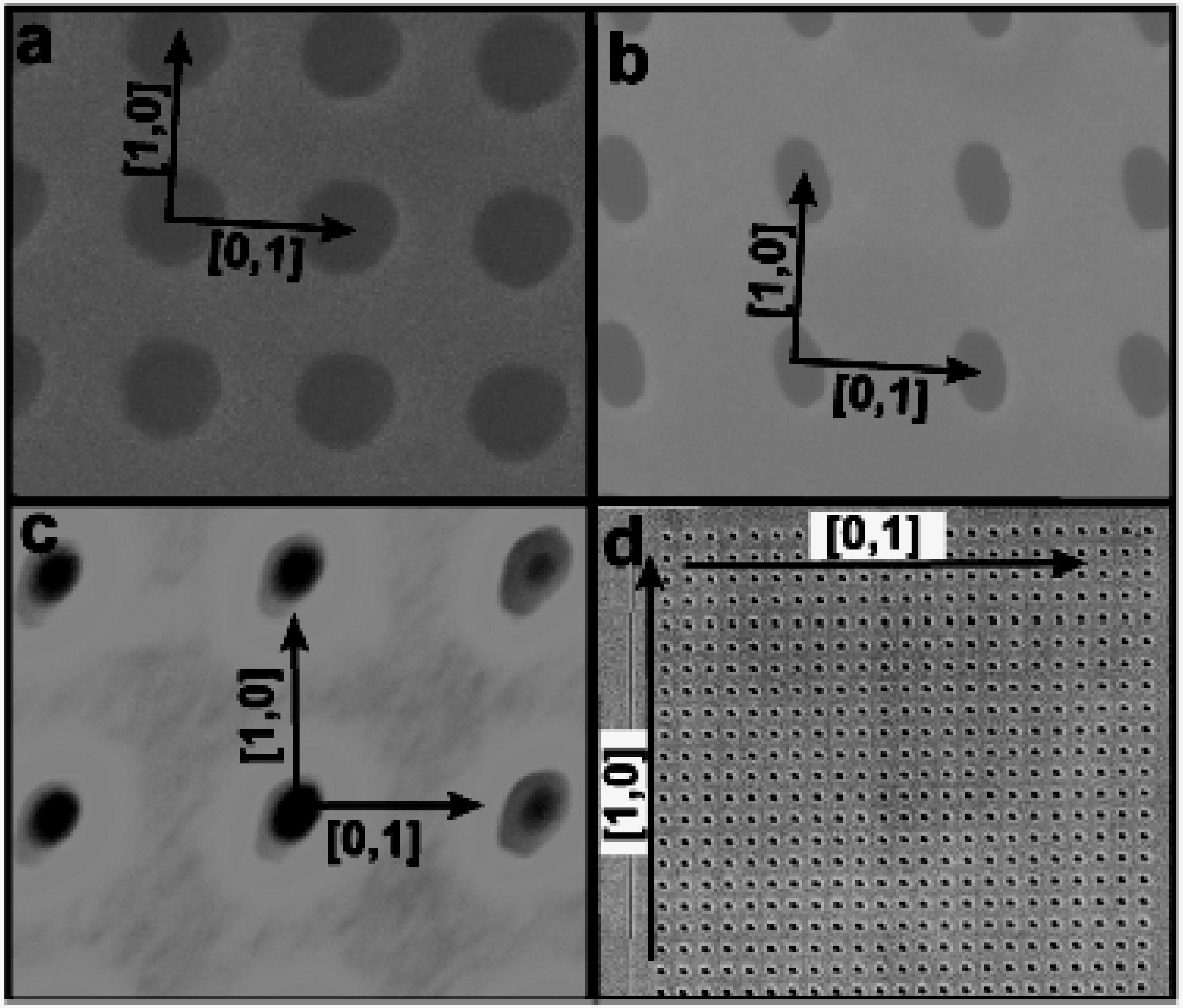

FIG. 1. Scanning electron micrographs of square nanohole arrays in gold. (a) Nearly circular holes. (b) Elliptical holes, 0.6 aspect ratio and major axis at $-12°$ to the $[1,0]$. (c) Elliptical holes, 0.6 aspect ratio and major axis at $33°$ to the $[1,0]$ axis. (d) An expanded view of (c) showing the full 16.1 μm wide array of 529 holes (holes spaced by 704 nm).

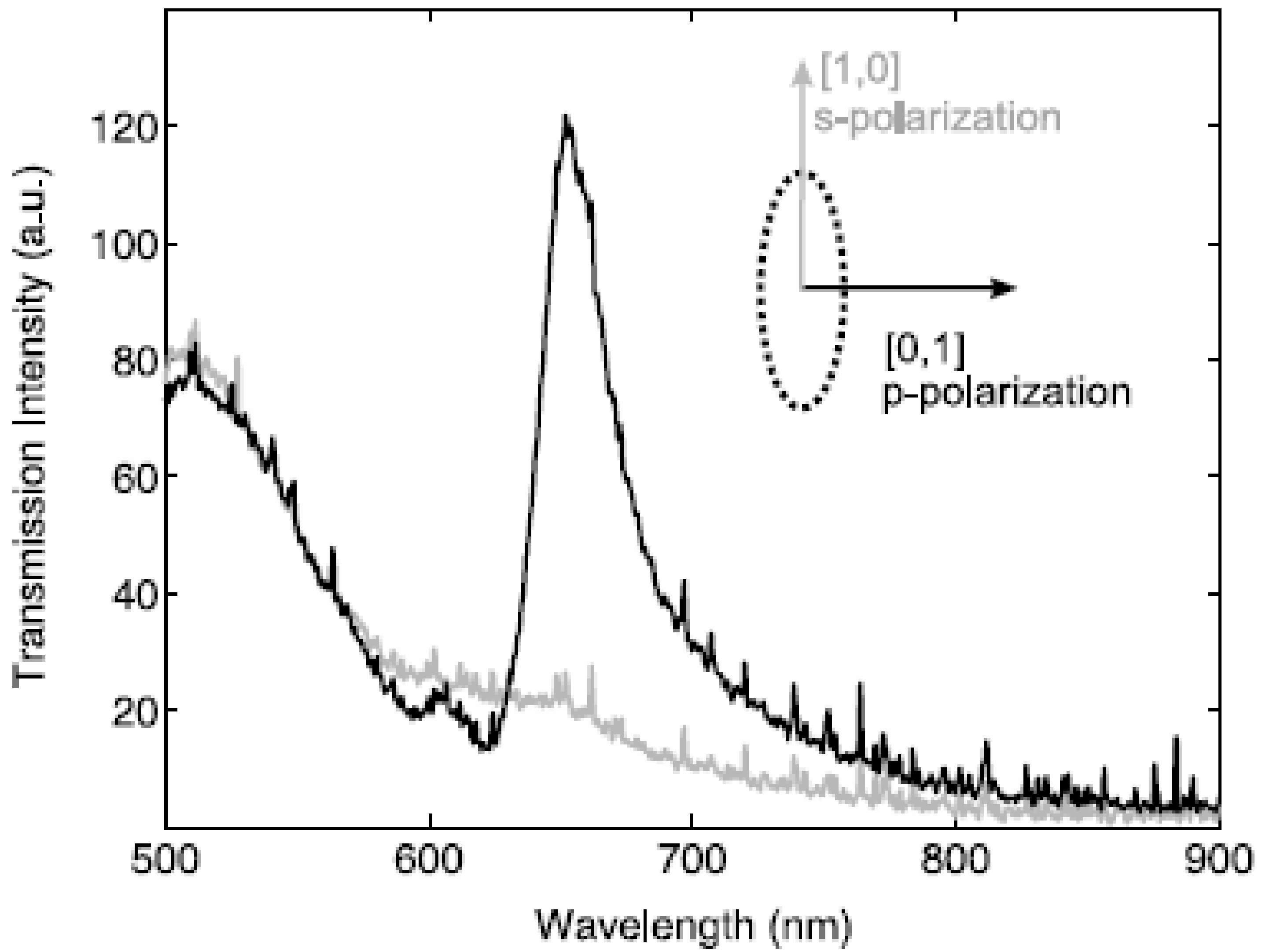

FIG. 2. Transmission spectrum through elliptical nanohole array for two orthogonal linear polarizations, with a 0.3 aspect ratio between the minor and major axes of the ellipse. The p polarization is parallel to the [0, 1] direction.

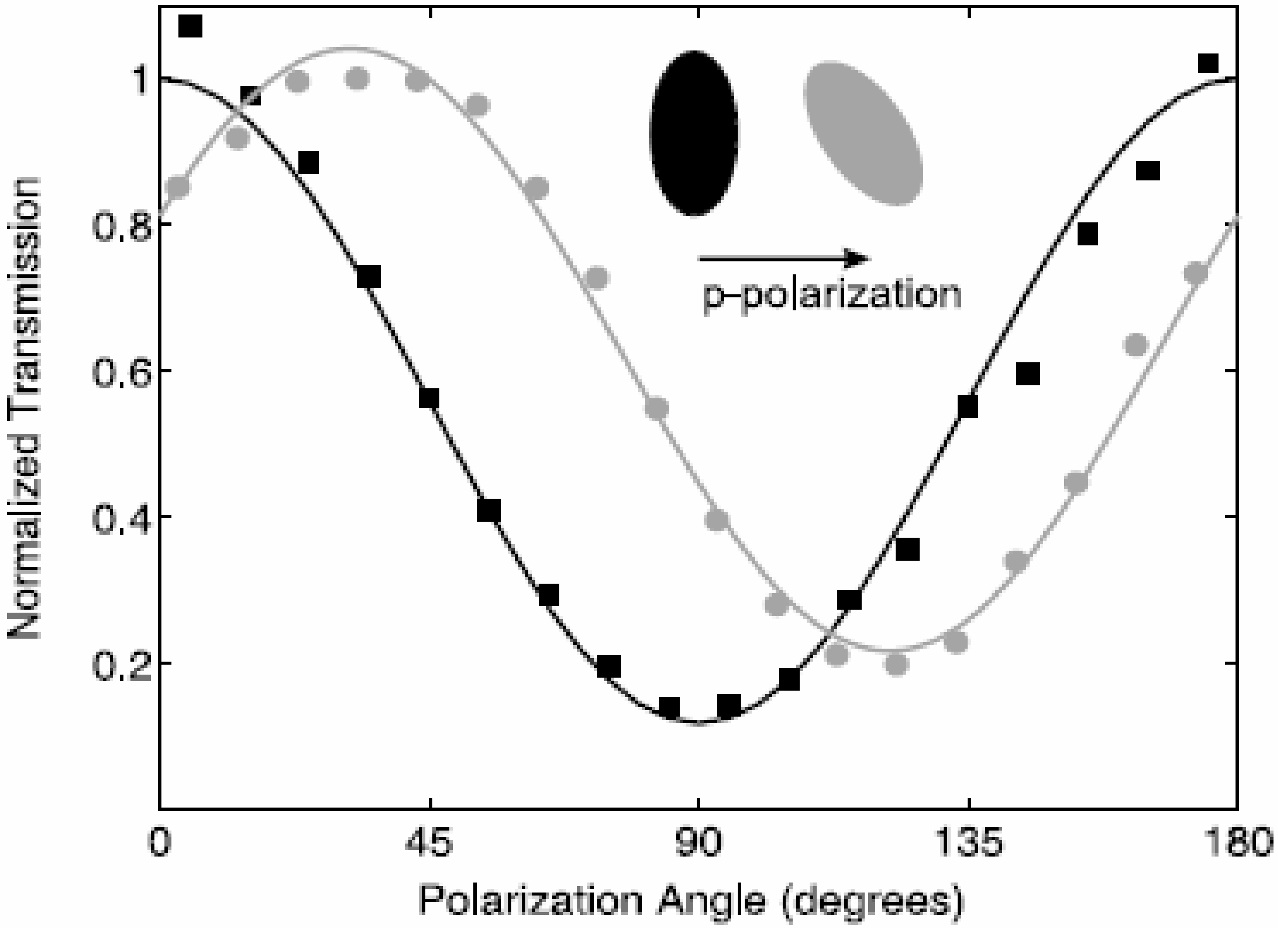

FIG. 3. Polarization dependence of transmission at the (0, 1) resonance peak, normalized to the maximum. Transmission shows cosine dependence when the major axis of the ellipse is oriented both at 0° and 33° to the [1, 0] axis of the array. The *p* polarization, along the [0, 1] direction of the lattice, corresponds to a polarization angle of zero degrees. The maximum transmission occurs for polarization perpendicular to the broad side of the ellipse.

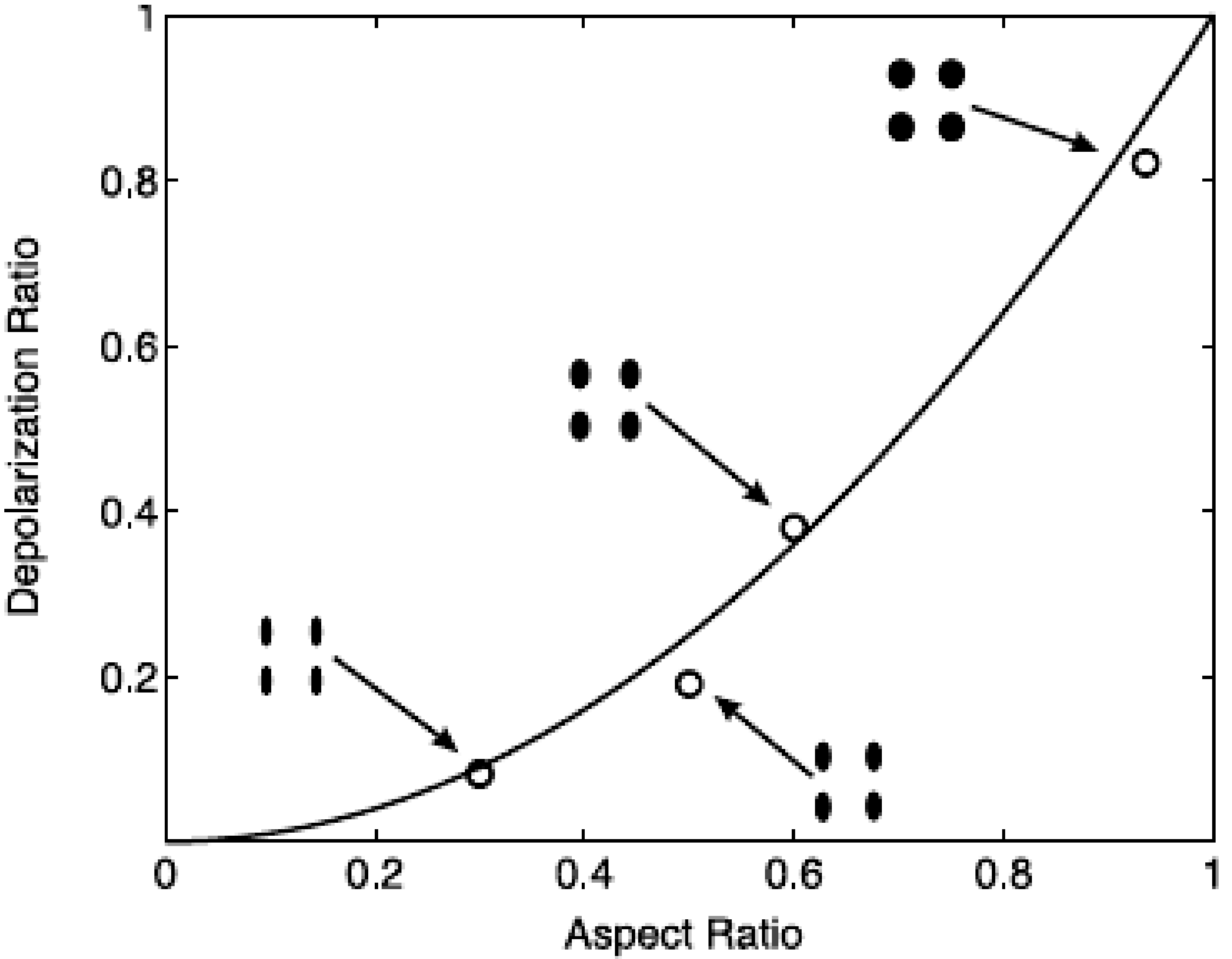

FIG. 4. The depolarization ratio of the transmitted light as a function of the aspect ratio of the holes. Solid line shows the $y = x^2$ curve.

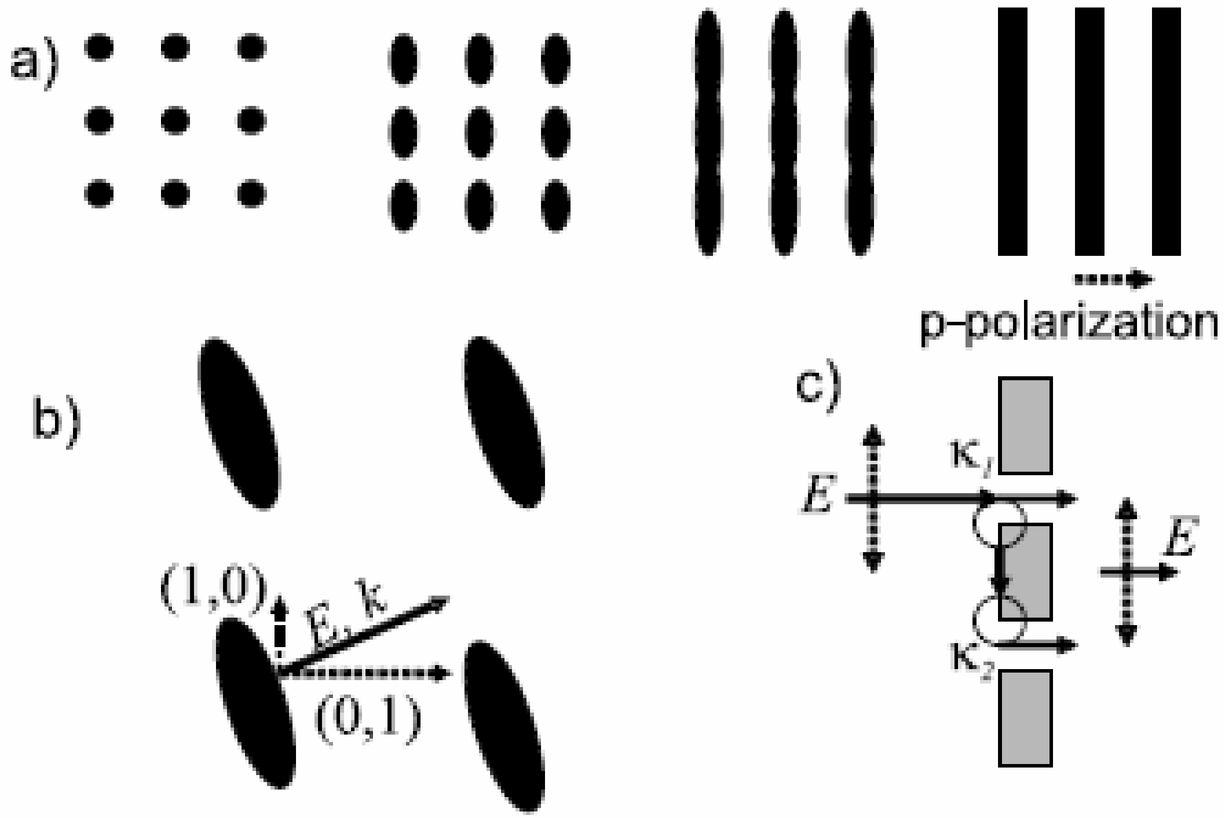

FIG. 5. (a) Elliptical holes approaching limiting case of slits, which only show enhanced transmission for p polarized light. (b) Enhanced SP excitation perpendicular to major axis of ellipse leads to preferential excitation of the $(0,1)$ resonance with respect to the $(1,0)$ resonance. (c) Coupling both into and out of the SP mode is required to obtain enhanced transmission from periodic array of holes, which results in a squared dependence of the enhanced transmission on the coupling strength.

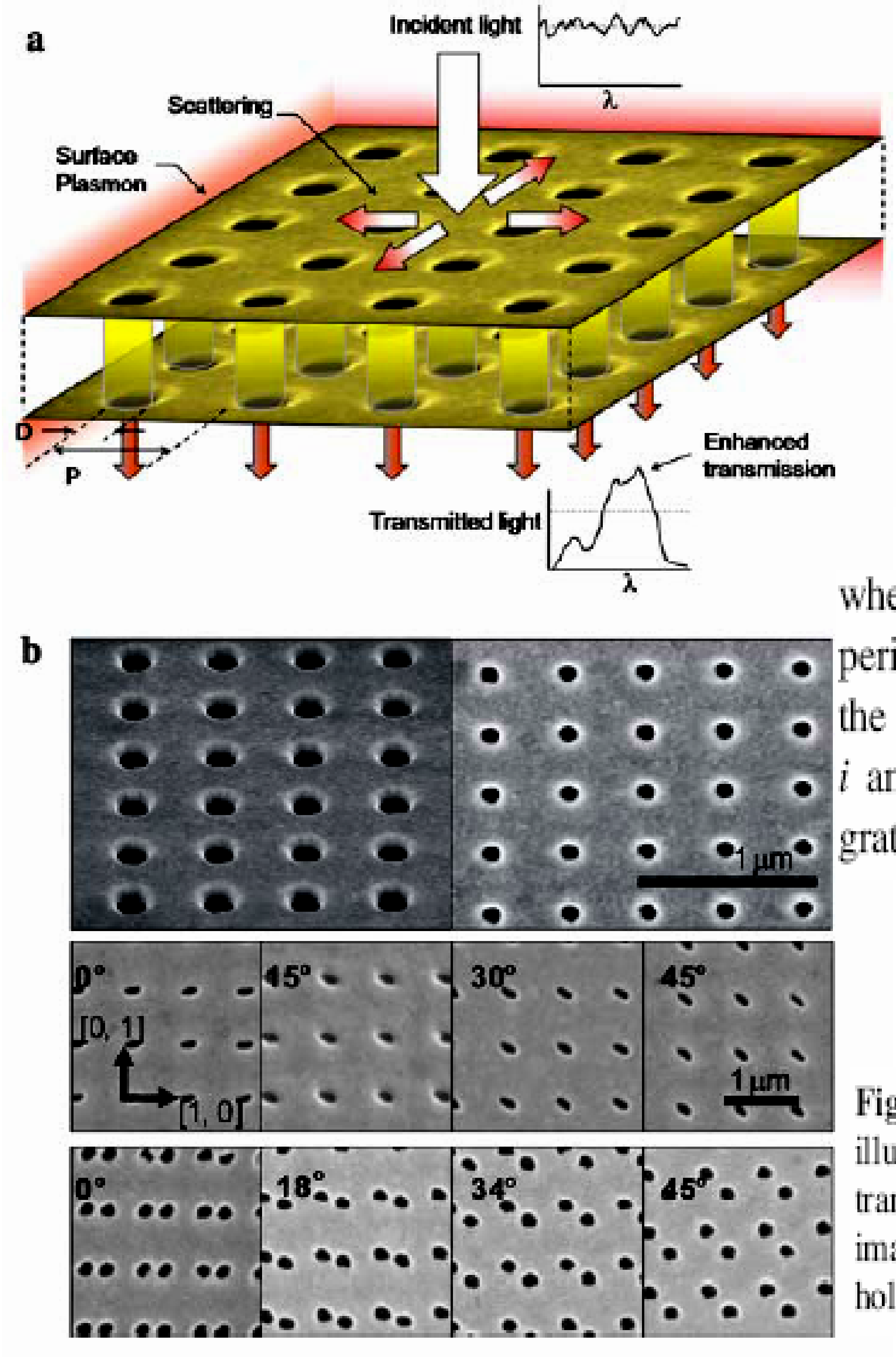

$$\lambda^{SP}(i,j) = p\left(i^2 + j^2\right)^{-1/2}\left(\frac{\varepsilon_d \varepsilon_m}{\varepsilon_d + \varepsilon_m}\right)^{1/2}$$

where the wavelength for coupling (λ^{SP}) is governed by the periodicity p of the array, ε_d is the relative permittivity of the dielectric, ε_m is the dielectric constant of the metal, and i and j are integers related to the scattering order of the grating.

Fig. 1 Nanohole arrays in metal films: **a** conceptual diagram illustrating incident light scattering into SP modes and enhanced transmission at select wavelengths; **b** scanning electron microscope images of several nanohole arrays of varying periodicity, and double-hole arrays with varying lattice orientations

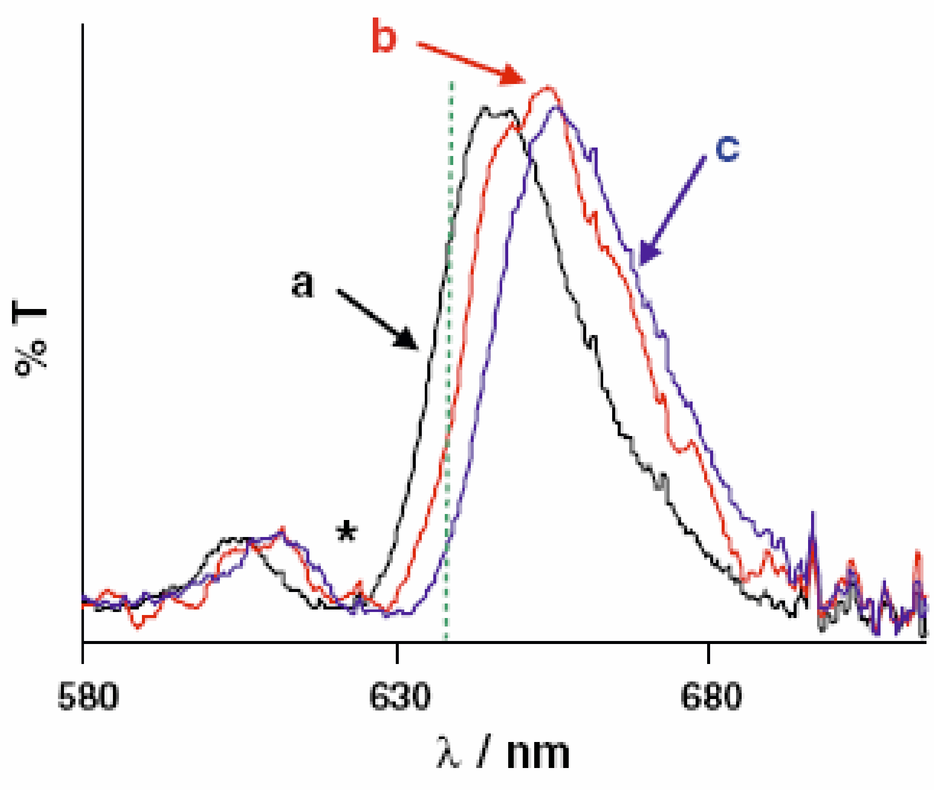

a bare gold surface; **b** gold with monolayer of MUA; and **c** gold-MUA layer with BSA.

Polarization dependent of biaxial nanoholes

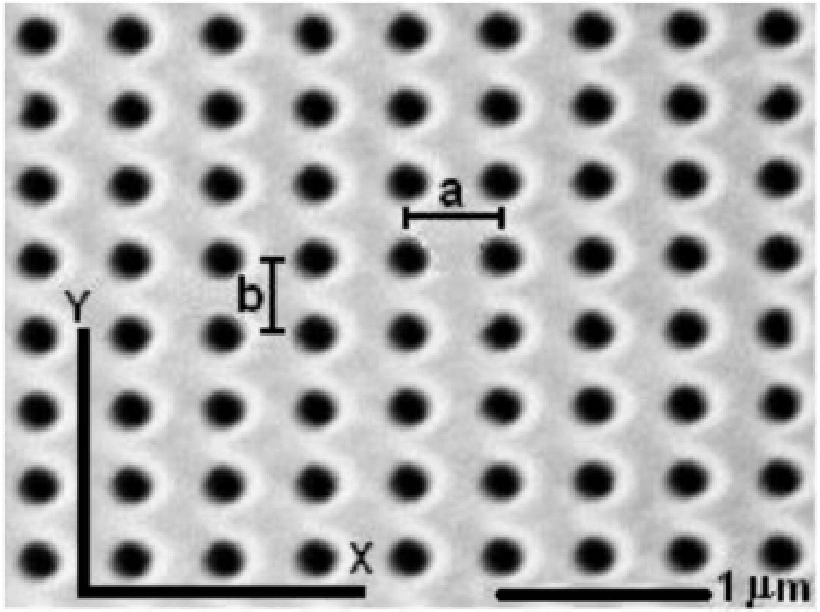

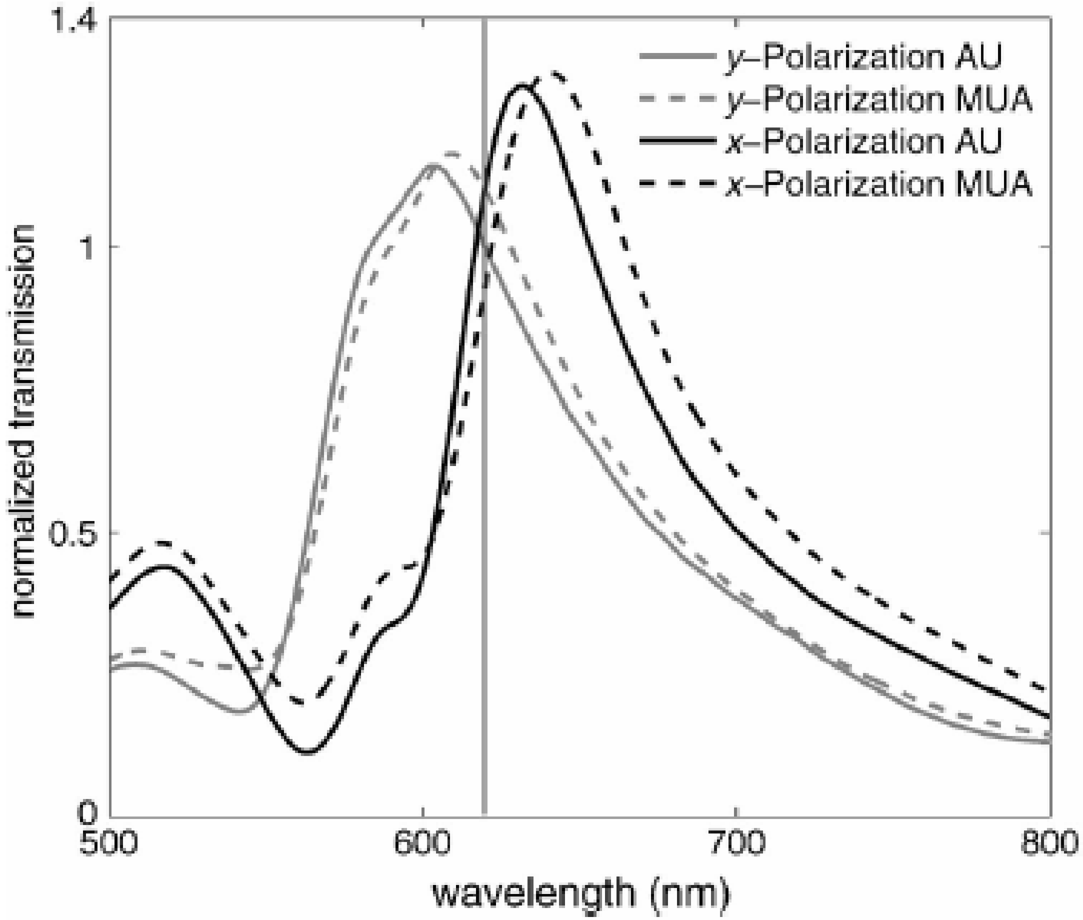

$$\lambda_{\max}(i,j) = \frac{ab}{\sqrt{i^2b^2 + j^2a^2}} \sqrt{\frac{\varepsilon_d \varepsilon_m}{\varepsilon_d + \varepsilon_m}},$$

Sensing with SPP

(a) Shown is a schematic diagram of the SPP imaging system. The array illumination is from a laser of wavelength $\lambda 0$ focused with a microscope objective. The resulting SPP mode is imaged on a CCD array using a 4F imaging system (MO and Lens). For the case shown, the incident +45° polarization is decomposed into orthogonal components that excite (1,0) modes at the array, which radiate in the forward and backward directions. The radiation is polarized at -45° to obtain the field in the image plane. MO1, MO2: Microscope objectives. ψP, ψA: Polarizer, analyzer angles. (b) Shown are spectral measurements of unpolarized zero-order transmittance for hole arrays in an aluminum film on a glass substrate. Data from arrays with different periods, a, were combined for the composite intensity image. The stitching frequencies appear as horizontal black lines, and data are replicated at negative wavenumbers for viewing. The SPP images correspond to four values of a/λ 0. The polarizer-analyzer pair was arranged at 0° /90° degrees for the ($\pm$1, $\pm$1) modes of the nanohole array with a/λ 0 = 1.41, and at +45° /-45° for the ($\pm$1,0) and (0,$\pm$1) modes for a/λ 0 = 1.03. Higher order modes were obtained at a/λ 0 = 2. No SPP excitation is observed for a/λ 0= 0.9.

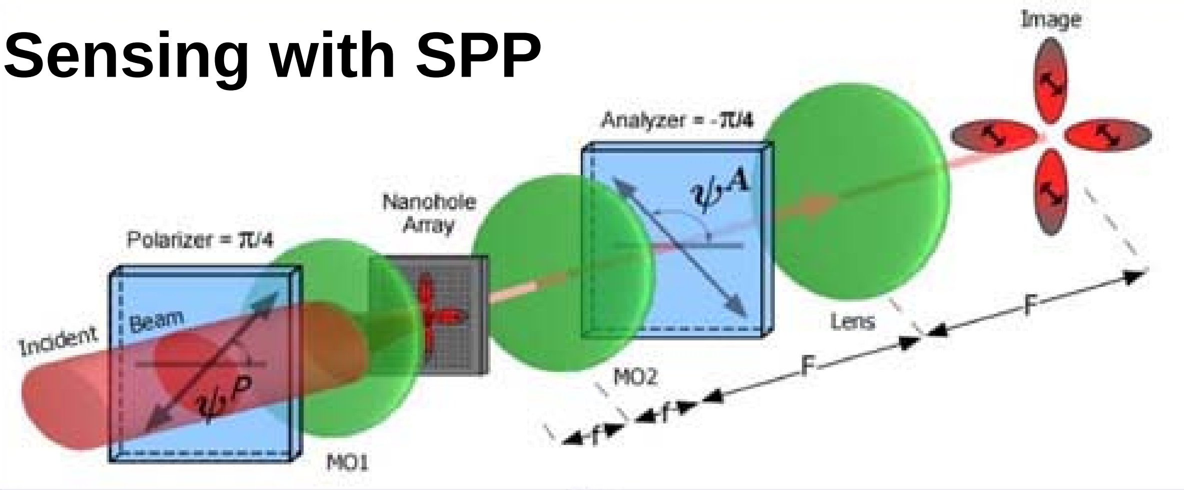

(a)

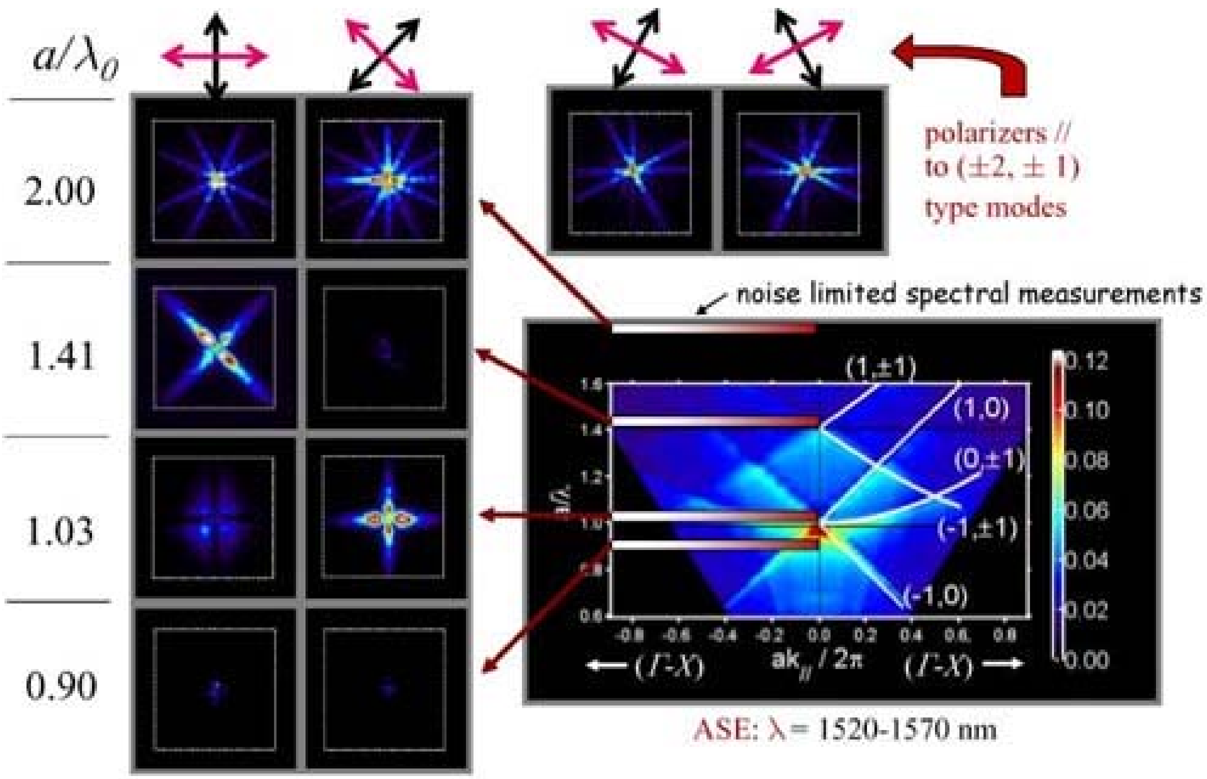

(b)

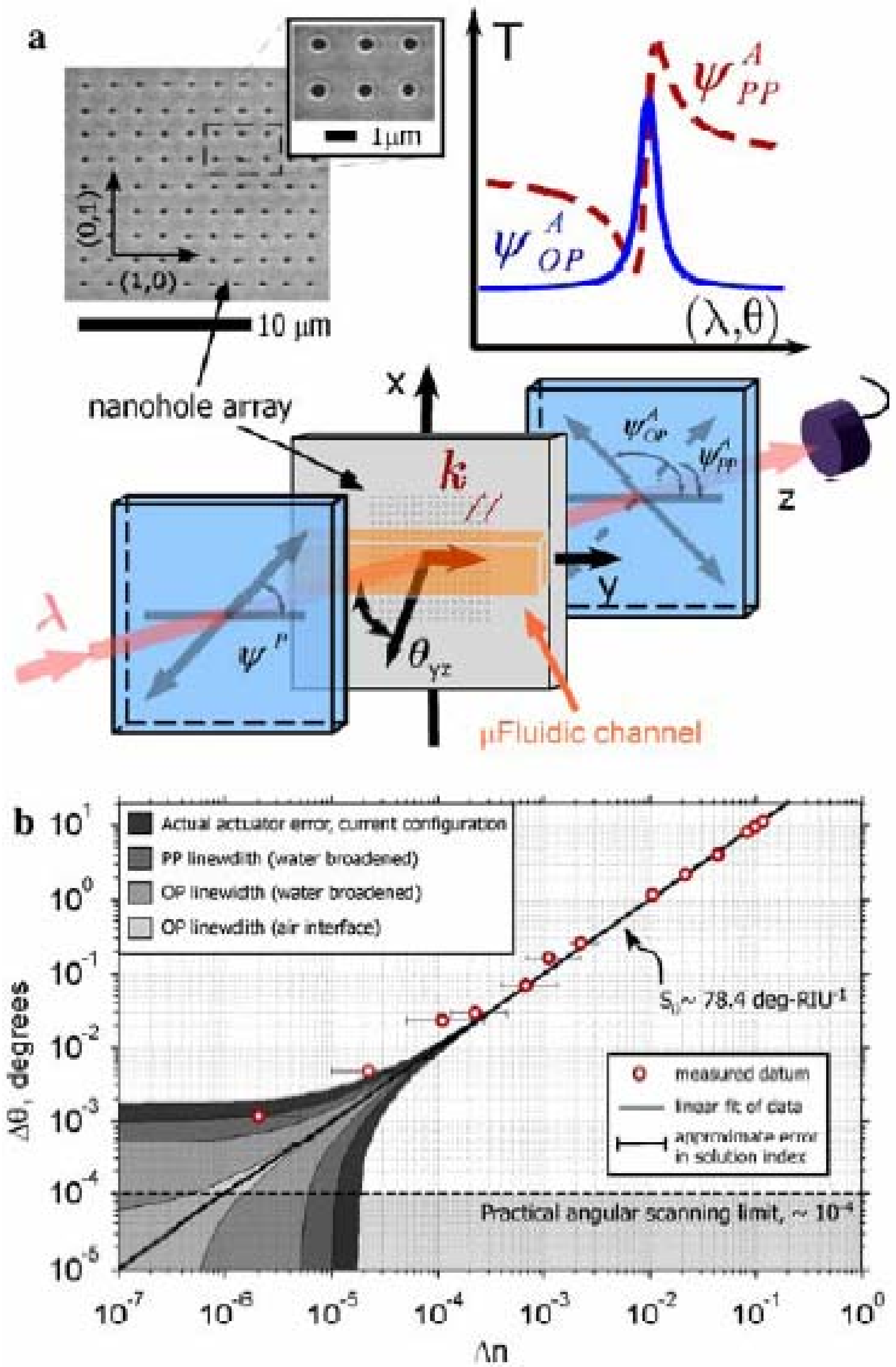

(a) Shown is a diagram of a 2D nanohole-array-based sensor. The input and output polarization states of a tunable laser are controlled, providing variable spectral or angular Fano-type profiles. A microfludic channel transports the analyte fluid to the surface of the sensing area, and can tune the SPP resonance frequency by controlling the refractive index at the metal-dielectric interface. Shown in the upper left are scanning electron microscope images of a representative sample. (b) The resonance-peak position shift is plotted versus the fluidic over-layer refractive index change, which depends on salt concentration. The black line is a linear fit to the log-log data. Δn: Refractive index change. θ : Resonant phase peak shift.

On-chip integration and application of nanoholes array

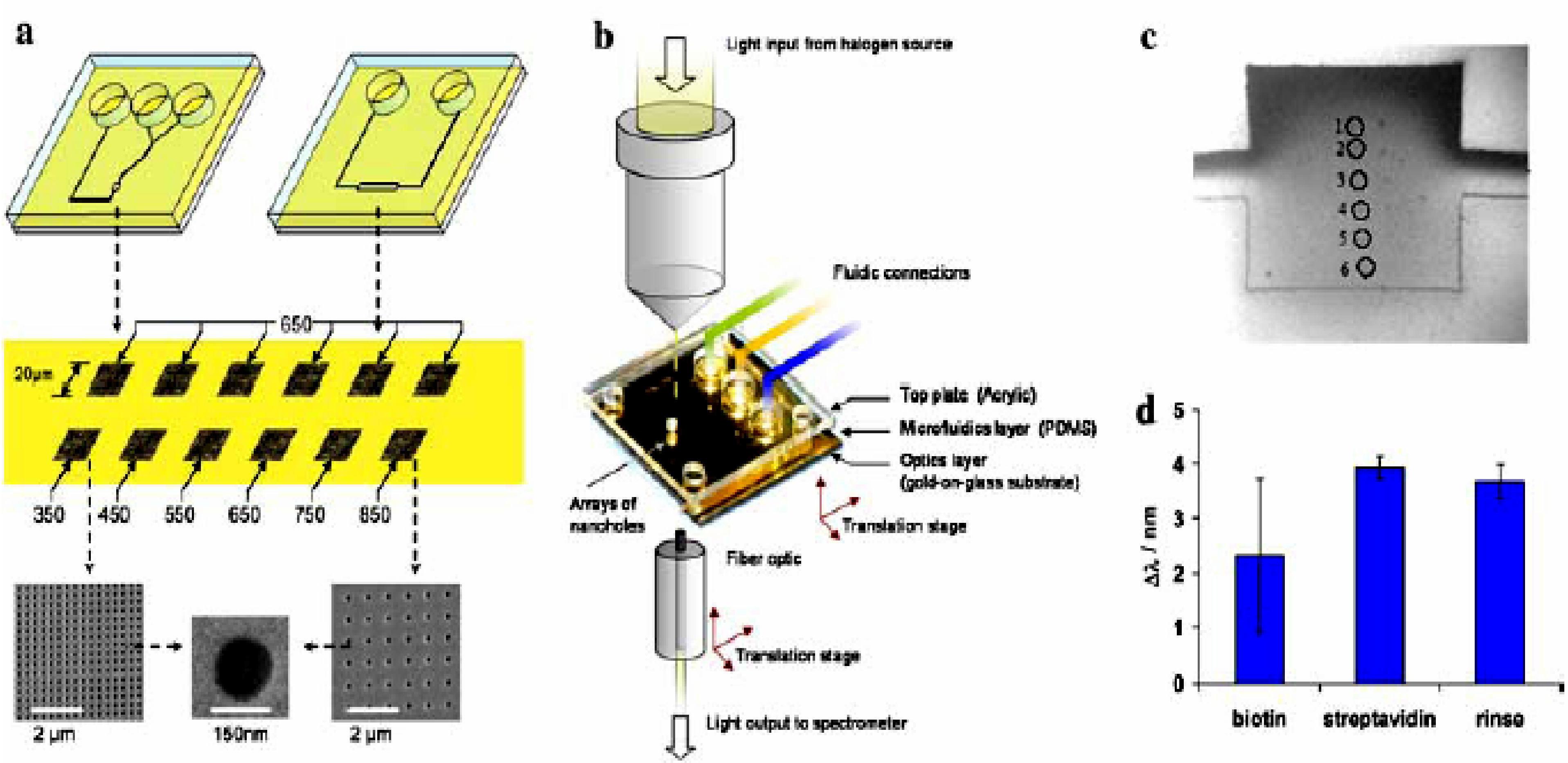

Optical trapping with nanoholes

Manipulation target:

- **cells, virus, DNA**
- **non-biological particles in fluidic**

Critical trapping distance from the surface, *d*

$$d = \frac{\lambda}{4\pi}\sqrt{\frac{n_m^2 + \varepsilon_m}{-n_m^4}}\ln\left(\frac{3\lambda^3}{16\pi^3 a^3}\frac{n_m}{\sqrt{-(n_m^2+\varepsilon_m)}}\frac{m^2+2}{m^2-1}\frac{I_x(0)}{I_z}\right)$$

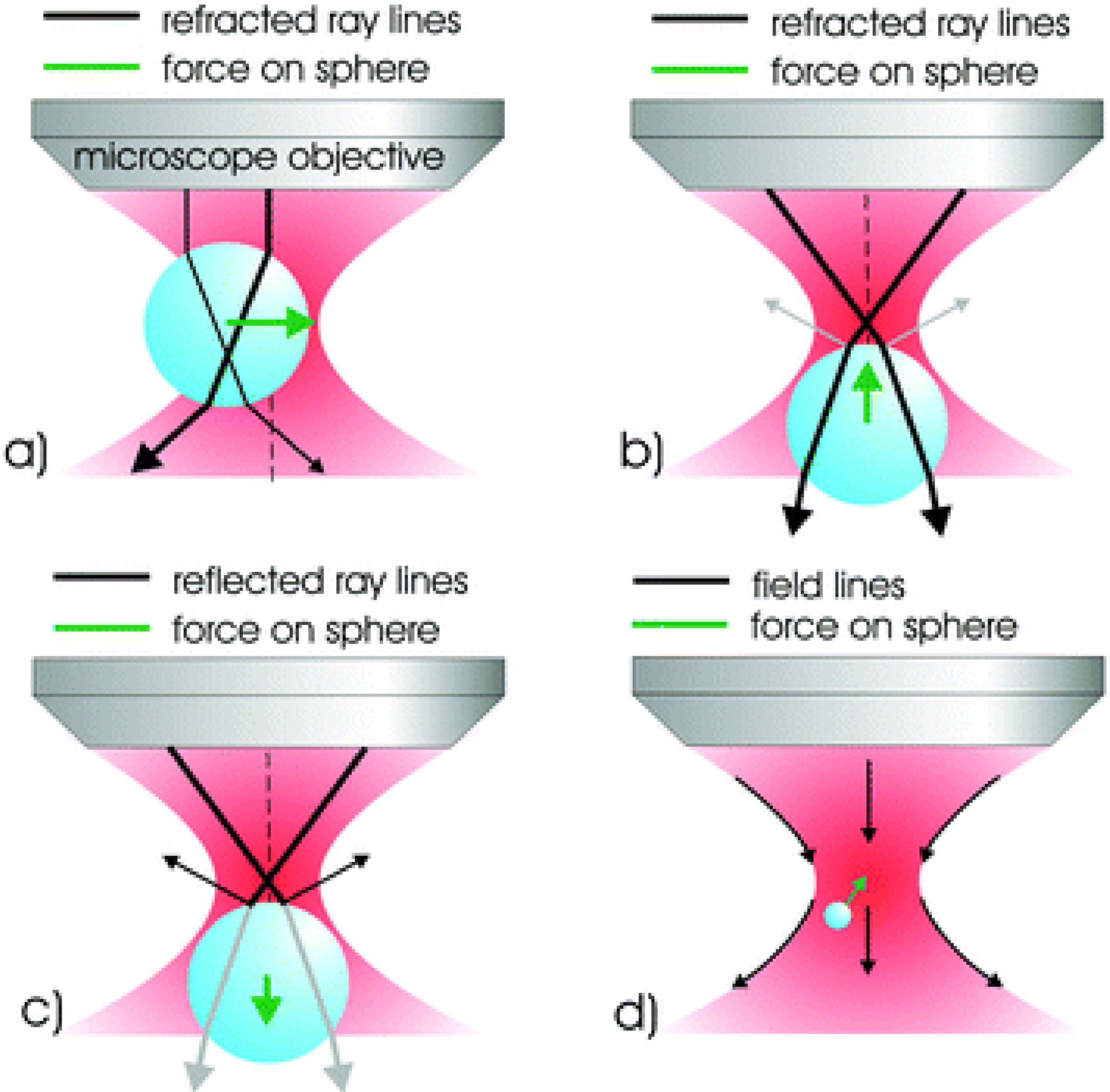

refracted ray lines
force on sphere
microscope objective
a)
refracted ray lines
force on sphere
b)
reflected ray lines
force on sphere
c)
field lines
force on sphere
d)

The polarization induced on the gold nanoparticle by a local electric field can then be written as

$$p(r) = \begin{pmatrix} \alpha_x & 0 \\ 0 & \alpha_z \end{pmatrix} E(r) \qquad (1)$$

Here, *x* and *z* are the polarizabilities along the *x* and *z* axes, respectively. In the data shown in Fig. 1b, *z*/ *x* is 1.18 at a wavelength of 780 nm, implying that the attached gold nanoparticle is slightly elliptical in shape

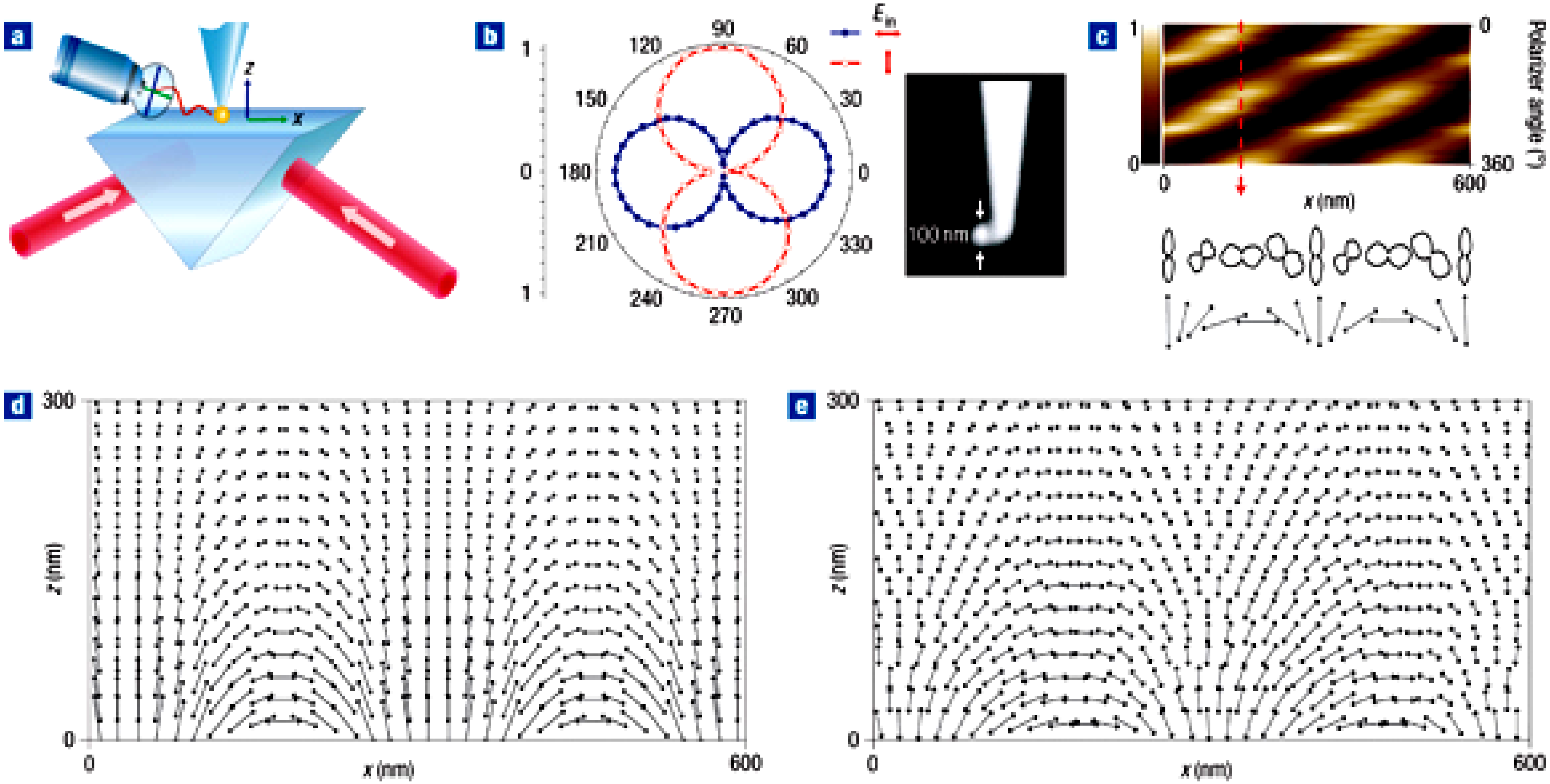

For an evanescent standing wave, generated by two counter-propagating *p*-polarized beams of equal intensity, the field vector is given by

$$\boldsymbol{E}(\boldsymbol{r}) = (E_x, 0, E_z) = E_0\left(\cos kx, 0, -\frac{k}{\kappa}\sin kx\right)e^{-\kappa z} \qquad (2)$$

where E_0 is a constant magnitude, k and   are related by the Helmholtz equation, k^2 = ($\omega/c)^2$, and are determined by the angle of incidence and the index of refraction of the prism.

The electric field of this standing wave can be written in the same form as equation (2), but now with a much larger *k*/ ratio equal to (- m) where m is the dielectric constant of gold:

$$\boldsymbol{E}(\boldsymbol{r}) = (E_x, 0, E_z) = E_0(\cos kx, 0, -\sqrt{-\varepsilon_m}\sin kx)e^{-\kappa z} \qquad (3)$$

***Nature Photonics* 1**, 53 - 56 (2007)

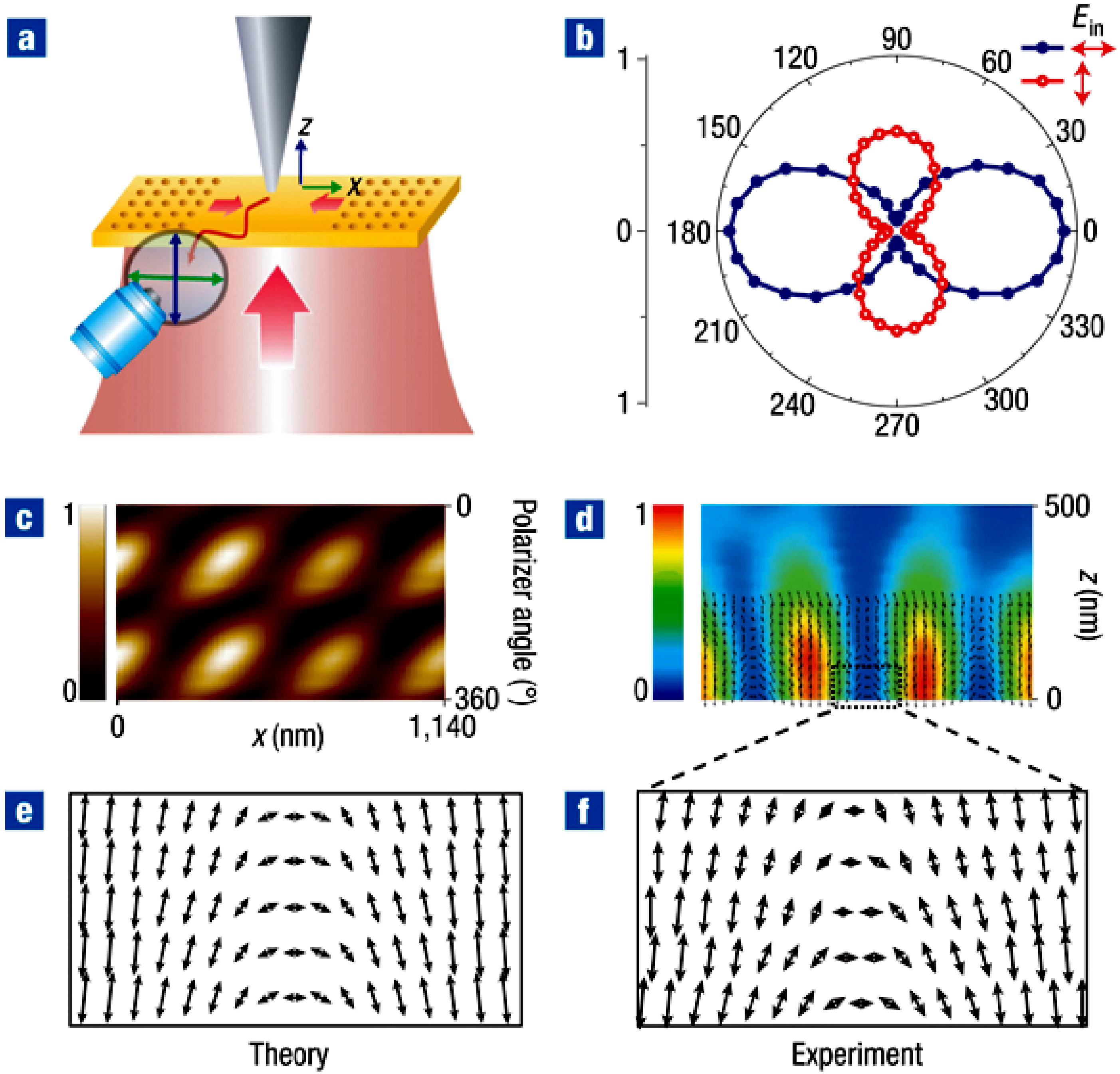

Figure 2: Vector-field mapping of the surface-plasmon polariton standing wave

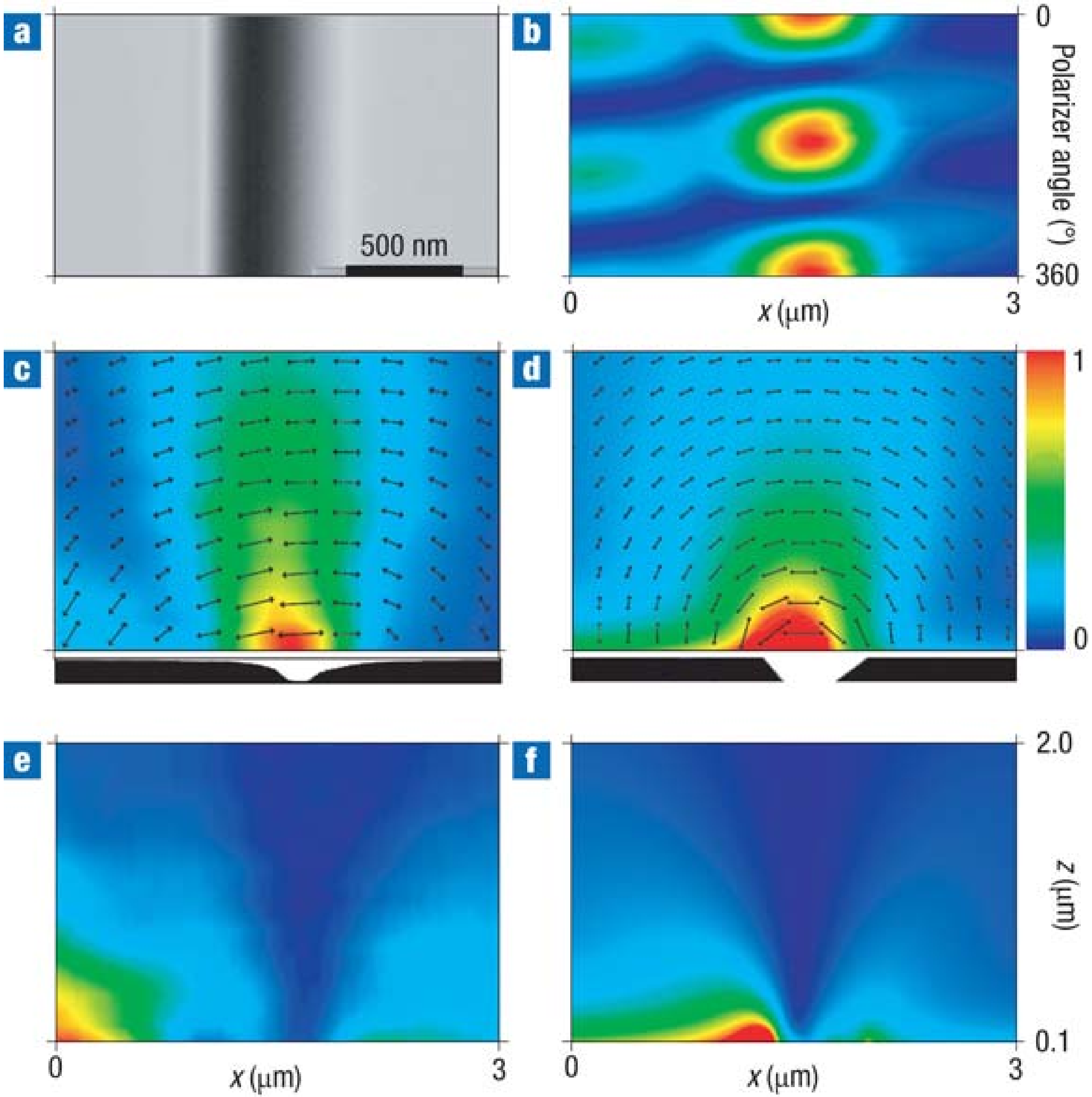

a, An SEM image of the single slit, showing the asymmetric slit shape. **b**, Constant-height scan image at z = 100 nm, rotating the polarizer by 360° . **c**, Vector-field image of a 3 m 2 m area starting from z = 100 nm, together with the total electric field intensity plot on a blue–red colour scale. At the bottom is shown an atomic force microscopic image of the slit profile. **d**, An FDTD calculation assuming an asymmetric trapezoidal slit shape. **e**, Experimental |*Ez*|2 plotted on a (different) blue–red colour scale. **f**, Theoretical |*Ez*|2 profile.

Figure 3: Vector-field mapping of light emerging from a single slit.

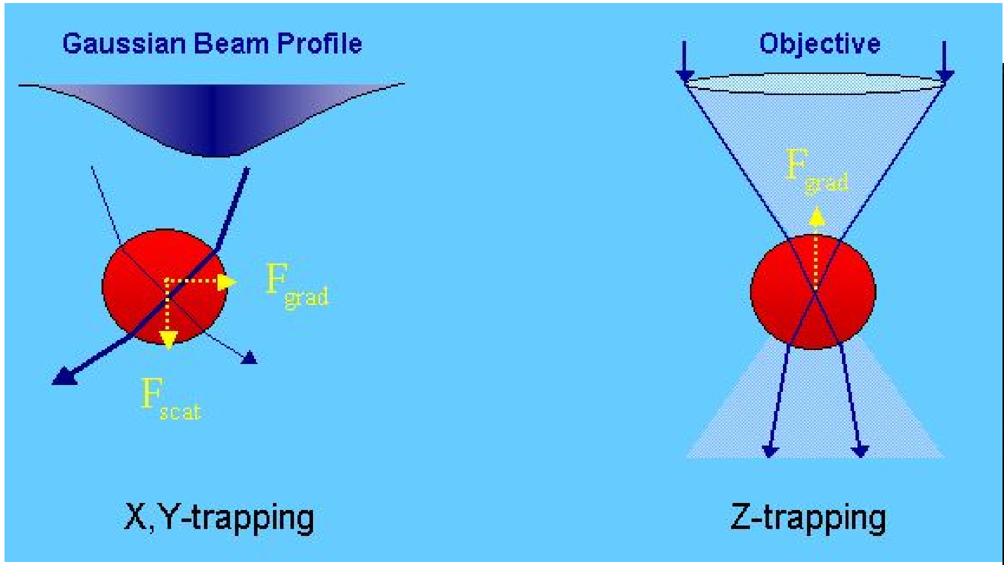

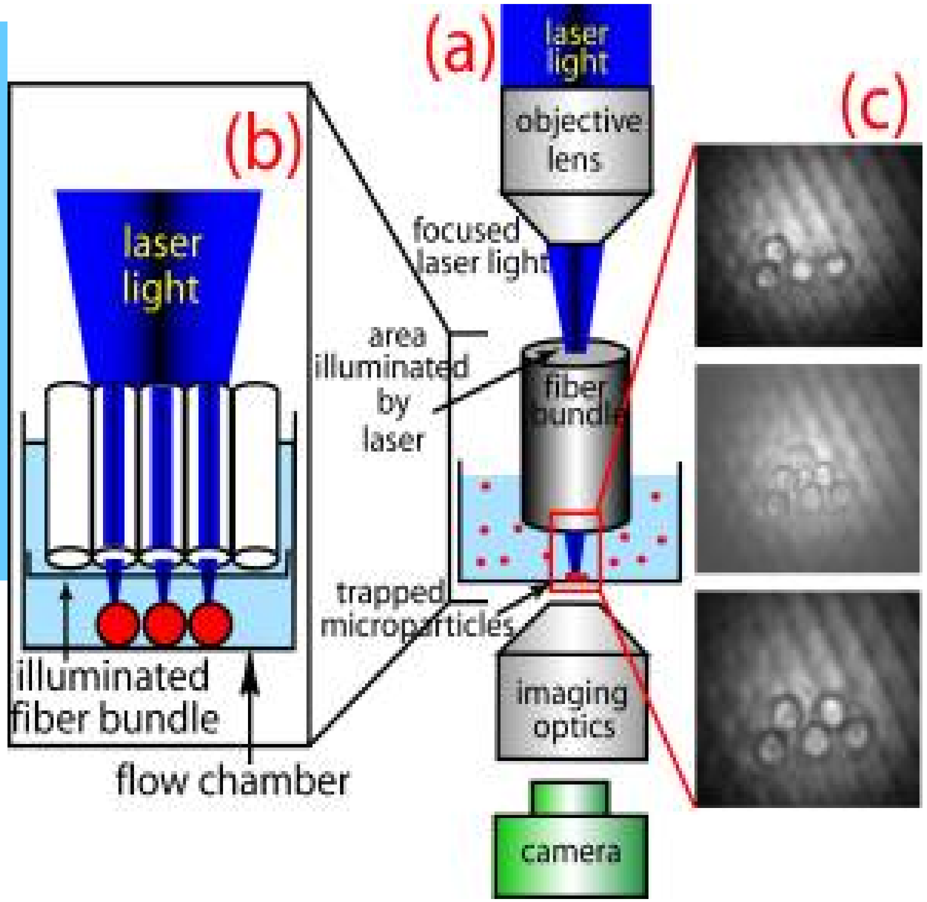

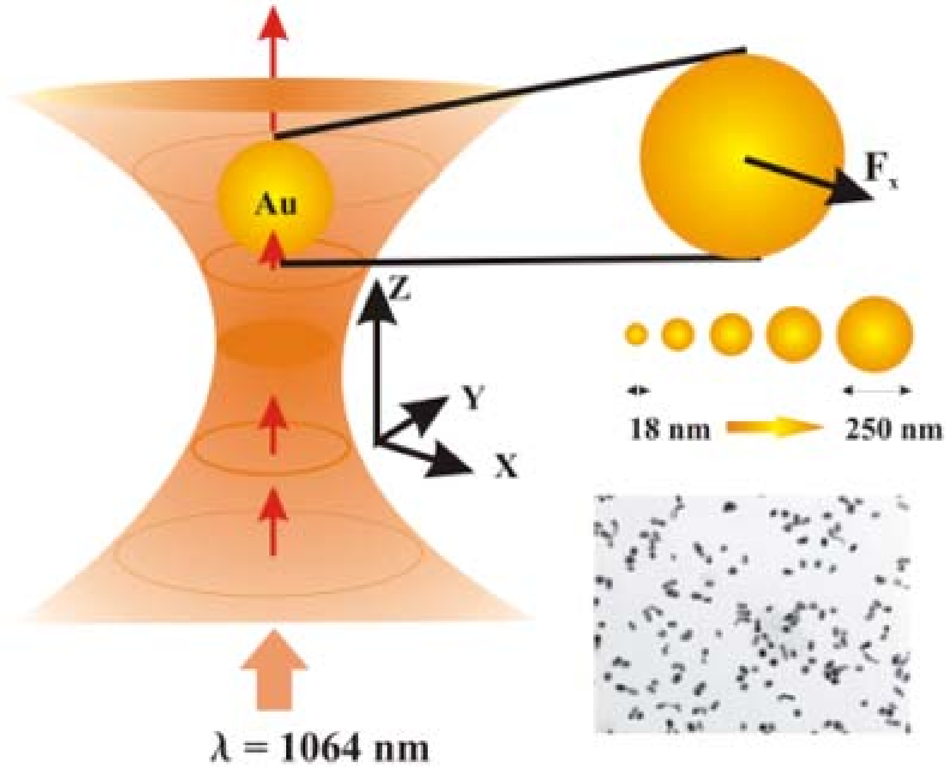

Optical trapping of gold nanoparticles

where λ is the wavelength of the light source, n_m is the refractive index of the medium in which the particles are suspended, ε_m is the real part of the dielectric constant of the metal, a is the particle radius, $m = \frac{n_p}{n_m}$ is the refractive index contrast, with n_p being the refractive index of the particle, $I_x(0)$ is the surface plasmon intensity at the surface of the metal, and I_z is the intensity of the transmitted light through the nanoholes. If the surface plasmon intensity is slightly higher than the transmitted light intensity, a trapping distance of 0.5 μm may be obtained

Practical plasmonic crystal biosensors

Images and schematic illustrations of a quasi-3D plasmonic crystal. (A) Scanning electron micrograph (SEM) of a crystal. (Upper Inset) A low-resolution optical image illustrating the diffraction colors produced by these structures. (Lower Inset) A high-magnification SEM that shows the upper and lower levels of gold. (B) Schematic illustration of the normal incidence transmission mode geometry used to probe these devices. The intensity of the undiffracted, transmitted light is monitored across the UV, visible, and near-infrared regions of the spectrum. (Inset) A close-up schematic illustration of the crystal.

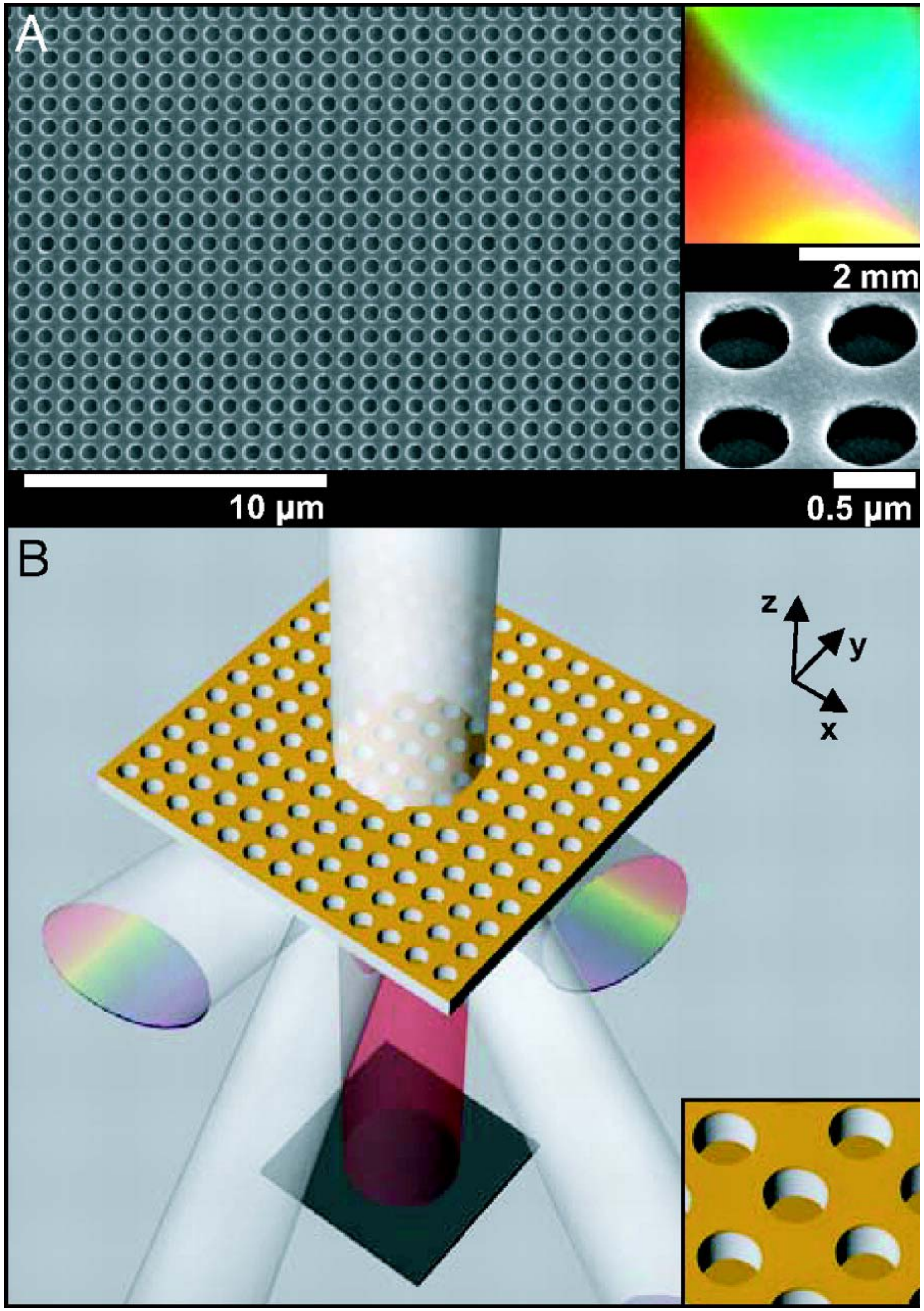

A hybrid plasmonic-photonic nanodevice for label-free detection of a few molecules

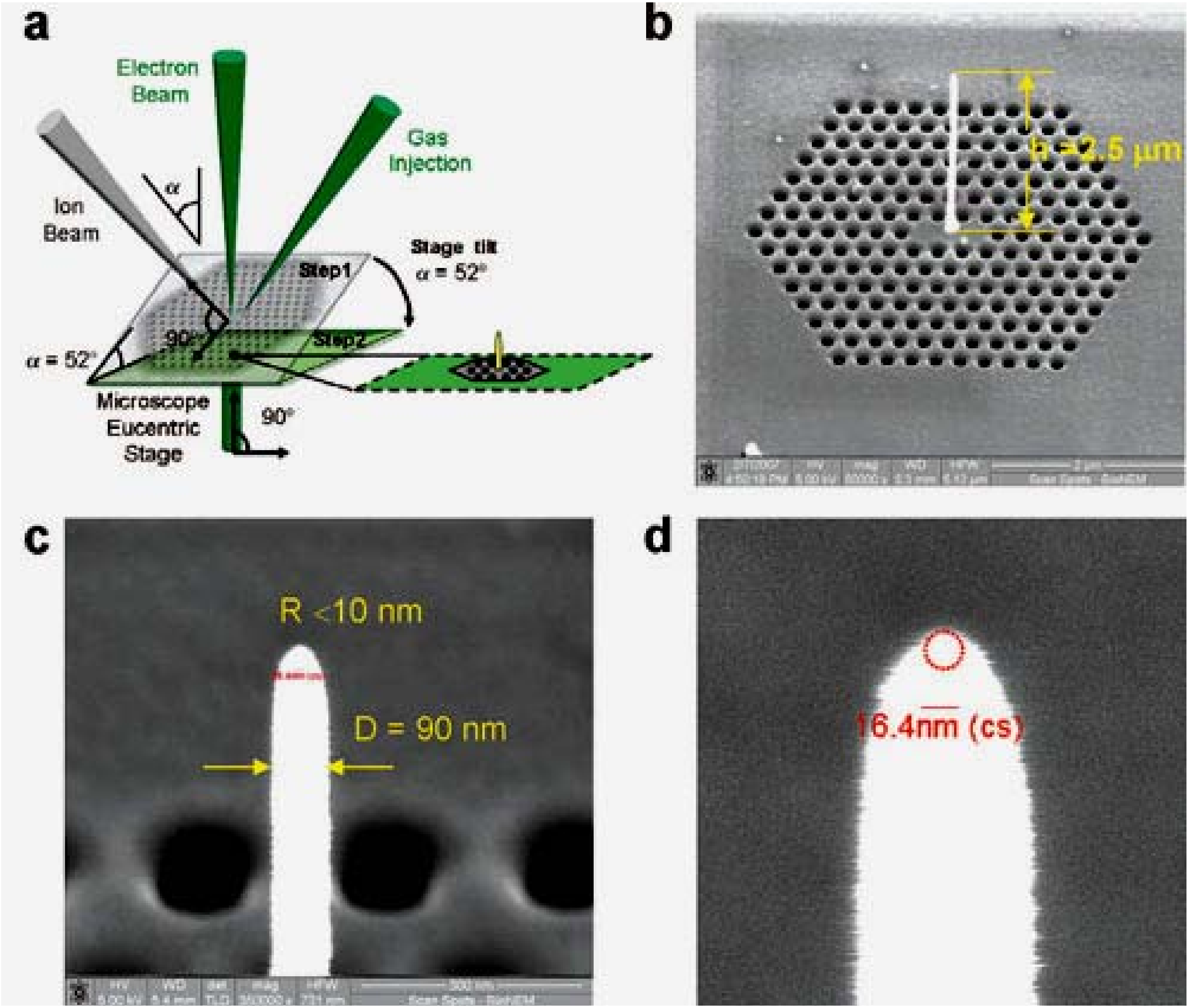

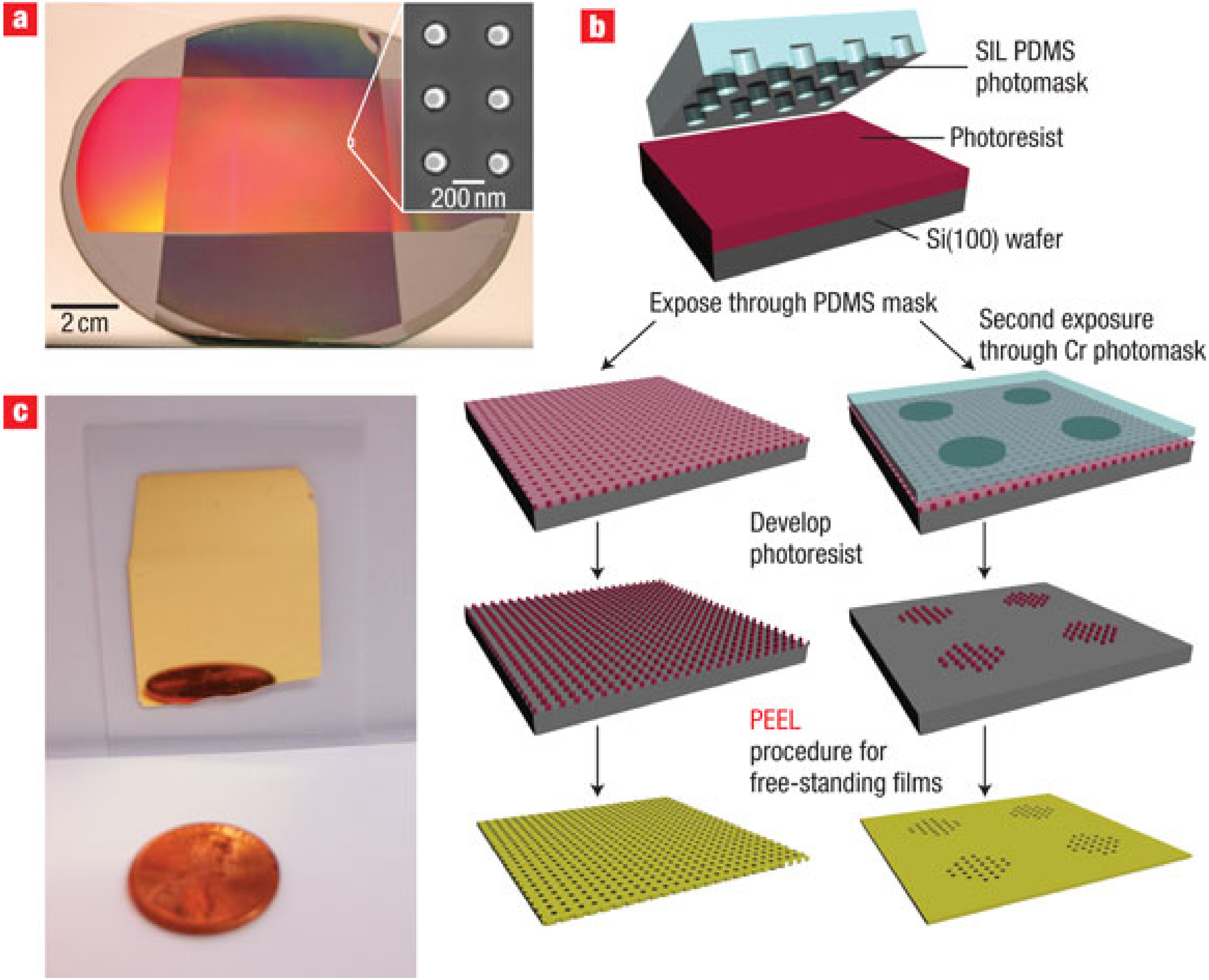
a
200 nm
2 cm
b
SIL PDMS photomask
Photoresist
Si(100) wafer
Expose through PDMS mask
Second exposure through Cr photomask
Develop photoresist
PEEL procedure for free-standing films
c

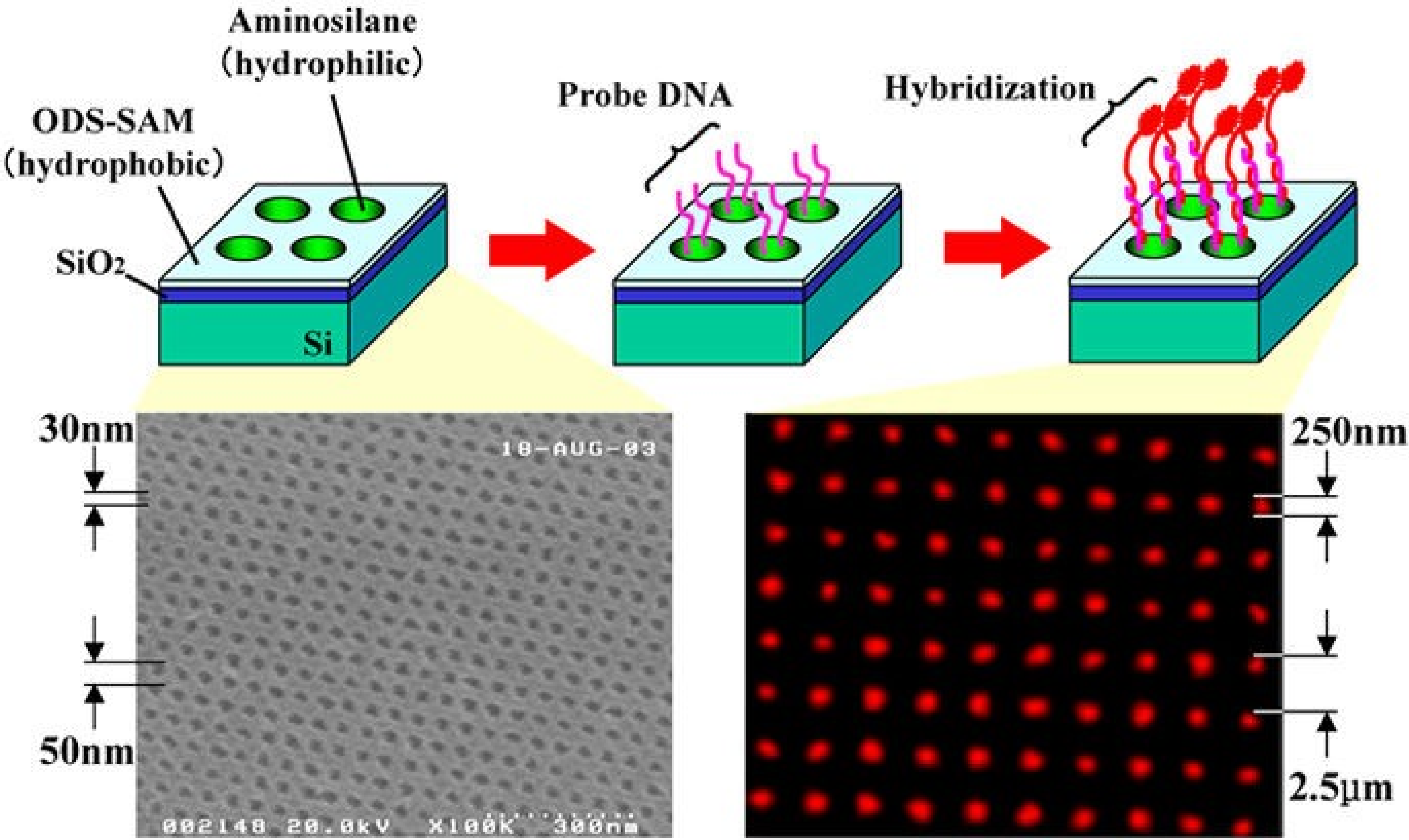

Fluorescence image of target DNA labeled with Cy-5 hybridized to the probe DNA immobilized within the nanostructured patterns by means of electron beam lithography onto organosilane self-assembled monolayer resist (Size:250nm, Pitch:2.5µm).

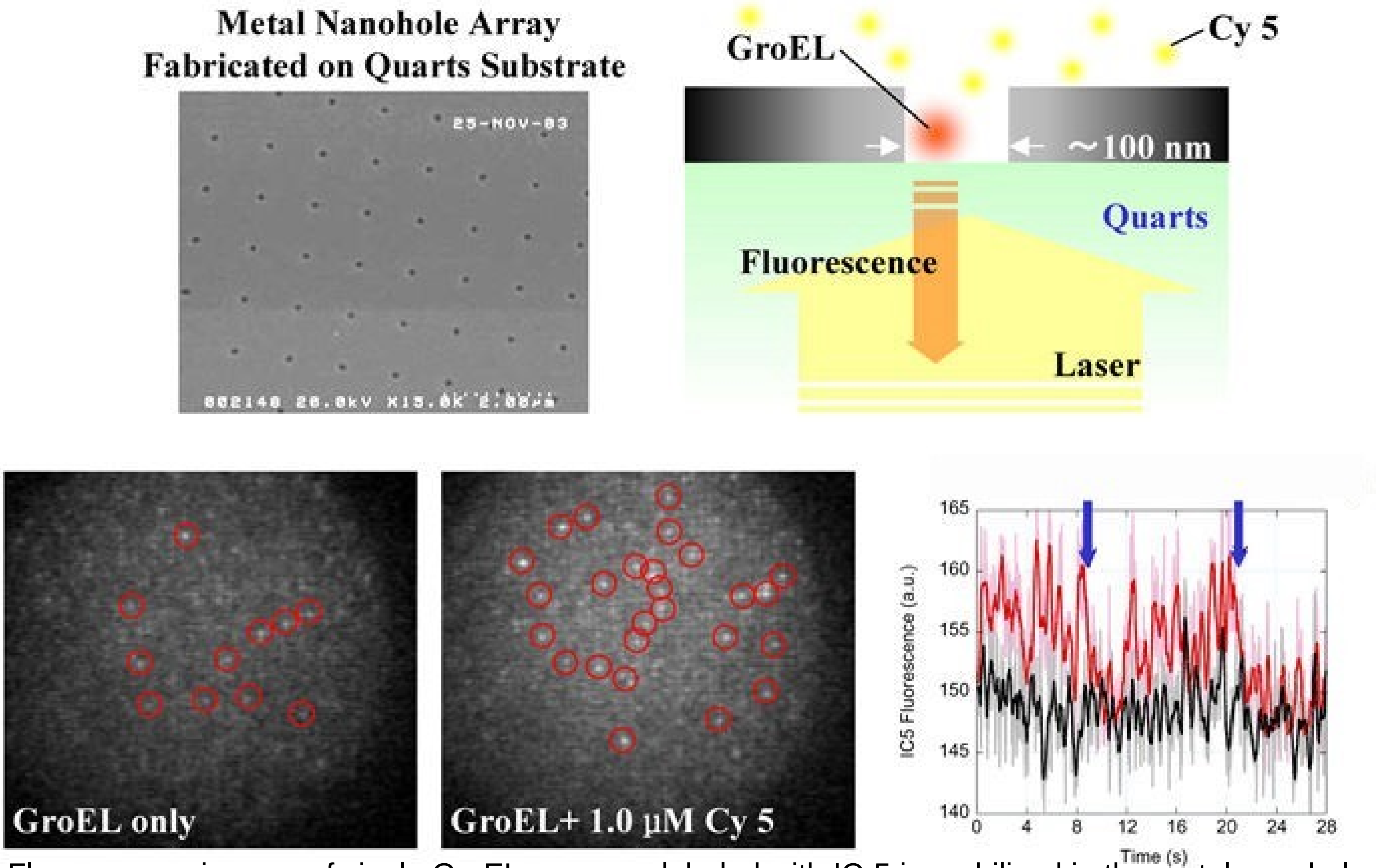

Fluorescence images of single GroEL enzymes labeled with IC-5 immobilized in the metal nanohole array on a quartz glass substrate. The quantized photo-bleaching proves the single molecule detection in each nanohole. The fluorescent dye Cy-5, which is diffused in water so that it mimics a protein in order to interact with GroEL, does not produce background noises because the laser light is guided only to the immobilized GroEL via the nanohole wave-guides.